JMEPEG (2005) 14:610-615
DOI: 10.1361/105994905X65016

1059-9495/$19.00

Indentation and Piercing of Steel in a Mushy State

J. Horský, M. Raudenský, P. Kotrbácek, and A.A. Tseng

(Submitted September 12, 2003; in revised form August 4, 2005)

Semisolid or mushy-state processing permits a material to partially solidify before shape-making operations. The understanding of material behavior in the mushy state is critical for better control of various semisolid processes. The aim of the current study is to experimentally quantify the indentation and piercing behavior of steel in mushy states. Semisolid specimens under indentation and piercing were evaluated at various forming speeds and mushy states. The correlation between the temperature and the percentage of the solid phase is used to control the characteristics of the mushy state. It was found that the forming resistance of steel in a mushy state is dependent on the deformation rate and the solid phase percentage.

Keywords forming, hot deformation, indentation, melting, mushy state, piercing, semisolid, steel

1. Introduction

Processing metals in a semisolid or mushy state has emerged as a vital commercial process for producing metal and metal-matrix composite components (Ref 1, 2). Among other benefits, it reduces the force requirement for the forging processes because lower flow stresses are involved. It also increases die life in die casting operations due to the lower temperature associated with the process. This process also refers to the casting of a metal that has been partially solidified under vigorous agitation so the dendritic structure is fully broken up. In addition, its viscosity can be varied over a wide range, depending on the processing conditions.

A great amount of work has been done in studying the semisolid structure and its rheological properties as well as the forming methodology. However, most of the work in the past has focused on the determination of material characteristics of relatively low-melting temperature materials, including aluminum, magnesium, tin, lead, and their composites (Ref 3-7). Due to the high-melting temperatures and other related measurement difficulties, there is a relatively small amount of experimental data available on steels. As a result, a testing apparatus that can accommodate with high testing temperatures was developed to study the indentation and piercing behavior of the mushy state steels.

The hot penetration tester has been used to perform experiments resembling both the indentation and the piercing processes. The steel specimens were evaluated at a wide range of solid to liquid ratios at various penetration speeds. Control of testing temperature is used to regulate the content of solid or liquid phase in mushy states. The changes in the percentage of these two phases are followed by changes in steel structures and rheology, which results in the change of the forming behavior. The dependence of forming force on penetration position at a constant penetration speed and temperature is the result of each measurement. A series of measurements were repeated for holding either the temperature or the forming speed constant.

J. Horský, M. Raudenský, and **P. Kotrbácek,** Fluid Flow and Heat Transfer Laboratory, Technical University of Brno, Brno, Czech Republic; and **A.A. Tseng,** Department of Mechanical and Aerospace Engineering, Arizona State University, Tempe, AZ 85287-6106. Contact e-mail: ampere.tseng@asu.edu.

Table 1 Chemical composition of steel sample

Element	Quantity, %
C	0.95-1.10
Mn	0.20-0.35
Si	0.30

2. Material and Microstructures

A high-carbon tool steel was selected for the present deformation study. Its composition is shown in Table 1. Due to the low content of elemental additions, the equilibrium binary phase diagram of Fe-C can be used to define the solidus and liquidus temperatures as well as the percentage contents of the liquid phase.

Based on the Fe-C phase diagram shown in Fig. 1, the solidus temperature for the steel tested was found to be approximately 1346 °C, and the liquidus temperature 1465 °C (Ref 8). These temperatures are consistent with the measurement data obtained by a separate test. The difference between the liquidus and solidus temperatures is 119 °C and the well-known lever rule is used to estimate the contents of the solid and liquid phases by providing the testing temperature.

The microstructures of the selected material were studied. Material samples were first heated to a specific temperature within the mushy state and then quenched to the room temperature in which the microstructure and percentage of solid phase at the instant of quenching can be preserved. The quenched samples were examined with both optical and scanning electron microscopes. Examination by a scanning electron microscope (Fig. 2) showed intercrystalline fracture after heating the steel sample to a temperature of 1430 °C. Visible melt

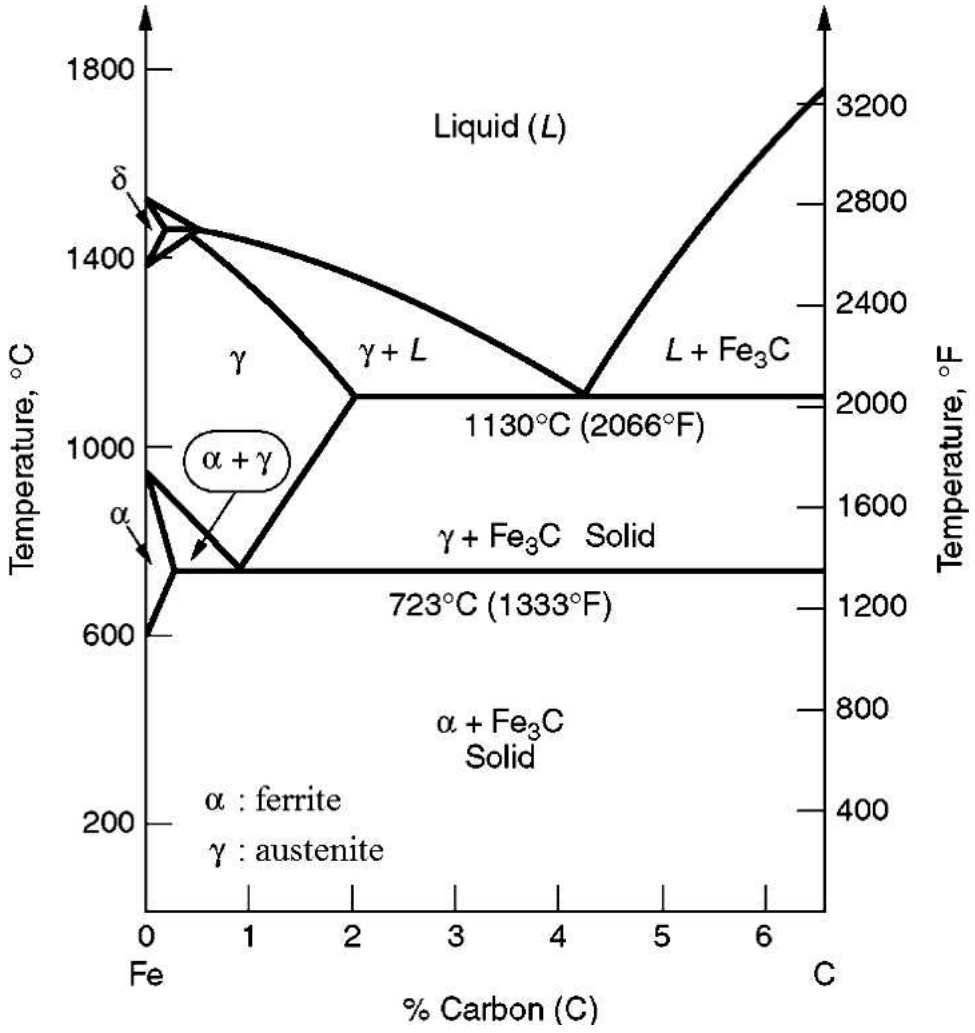

Fig. 1 Iron-carbon metastable phase diagram

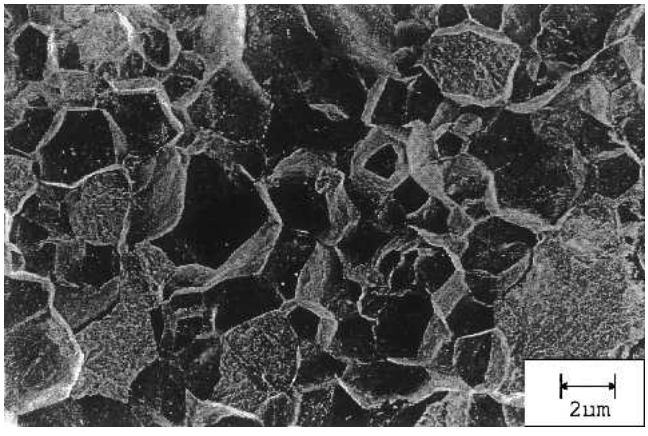

Fig. 2 SEM image of quenched sample

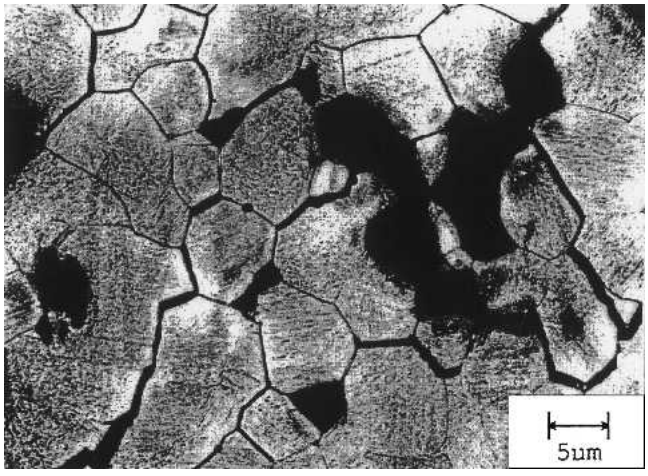

Fig. 3 Optical micrograph for quenched sample

down of grain boundaries prior to quenching was observed. Figure 3 shows the corresponding optical micrograph for a sample exposed to 1430 °C for 1 h before quenching.

The flow stress of the selected steel at the mushy state was recently studied. Tseng et al. (Ref 9) used the hot compression test to develop the relationship between the flow stress and the solid fraction. The solid fraction is defined as the weight percentage of solidus component in a mushy state. They found that the flow stress increases exponentially as the solid fraction increases and can be correlated as:

$$\sigma_f = A \exp(B f_s) \quad \text{(Eq 1)}$$

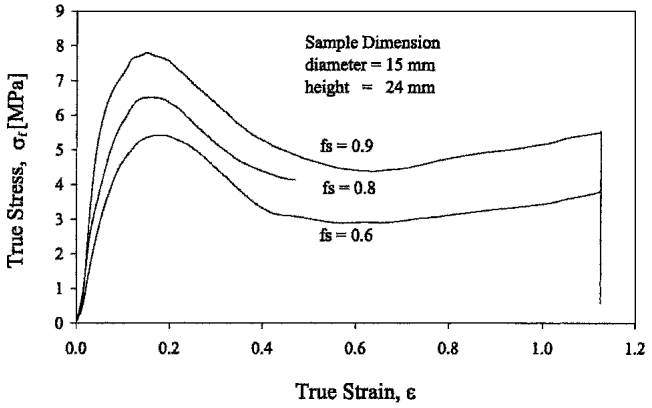

Fig. 4 Effects of solid fraction on peak flow stress of high carbon tool steel

where σ_f is the flow stress, f_s is the solid fraction, and A and B are the correlation constants. If the peak stress is selected as the flow stress, the correlation constants A and B are 2.66 and 1.17 MPa, respectively. These correlation constants can be directly extracted from the stress-strain curves displayed in Fig. 4, as reported by Tseng et al. (Ref 9). As shown, the peak stresses can be easily identified within a region having a strain between 15 and 20%, dependent on the specific value of the solid fraction. Based on the correlation, the peak stress at the solidus temperature, i.e., the solid fraction equal to 1.0, can be found to be 8.5 MPa. This solidus peak stress represents the possible maximum stress that can occur in the steel considered in mushy states. It will be used in normalization of the forces or loads obtained from the present indentation and piercing experiments.

3. Apparatus and Testing

The apparatus used for the indentation and piercing tests has been specifically designed to accommodate the high temperatures required to melt the steels. As shown in Fig. 5, it consists of an Instron load frame equipped with a position measuring device and a dynamometer with a range of up to 2 kN. A furnace specially designed to melt steel is situated within the load frame. The furnace is heated by two resistive heating elements placed at opposite ends of the furnace enclosure. The sample is placed in a ceramic crucible on top of the refractory concrete base between the two heating elements. The indentation or piercing tool is made of ceramics and can easily slide down the crucible to allow penetration. The design of the setup enables the steel sample to be accessed from both the top and bottom sides. The schematic diagram showing the major components of the apparatus is depicted in Fig. 6.

A control thermocouple is placed either close to the material sample, or inside the ceramic tool, to ensure that the preset temperature is achieved. Temperatures monitored from either location have been consistent with each other. Two different ceramic tools (indenter or punch) are used for the penetration of the steel sample while it is in a mushy state. A microcomputer-based data acquisition system collects information from the dynamometer and records position while the experiment is performed.

The sample is first placed in the furnace and heated to the temperature that corresponds to the meltdown point. The

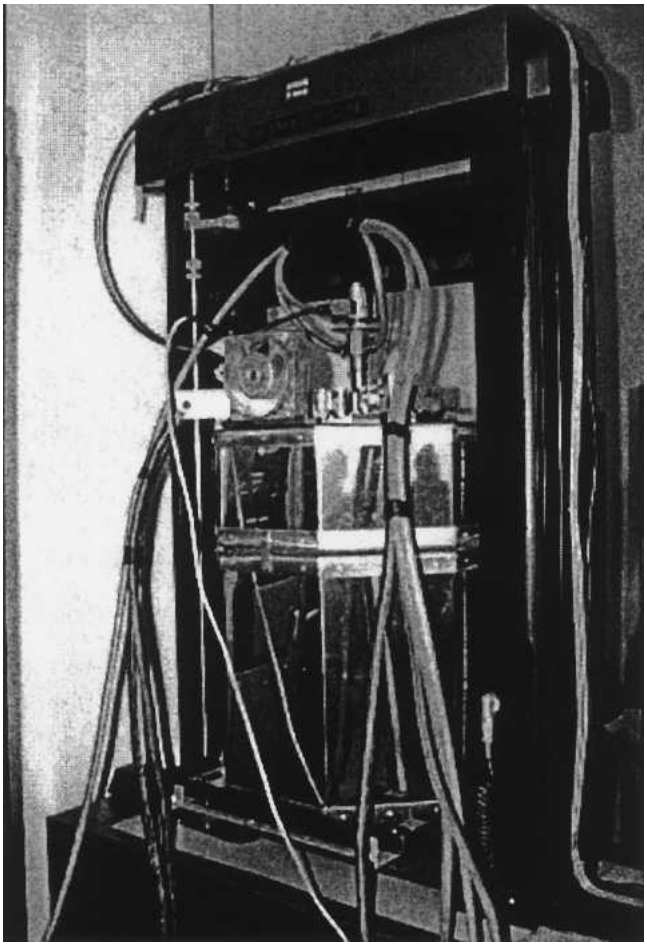

Fig. 5 Experimental apparatus for hot penetration tests

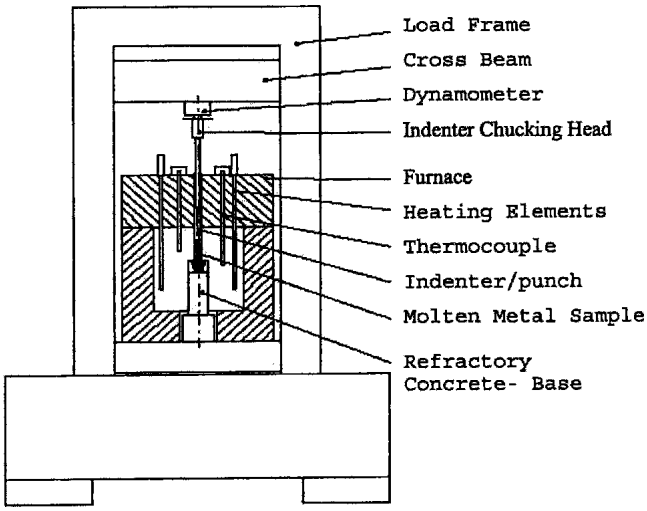

Fig. 6 Schematic diagram of penetration testing apparatus

temperature in the furnace is then decreased to the value prescribed for the particular experiment. Following that, the ceramic tool is pushed into the sample with the chosen speed of motion while the data describing the instant position of the tool and the instant force acting on the tool are monitored and recorded. The sample is then heated to the temperature where the liquid state is reached. Now the motion is reversed and

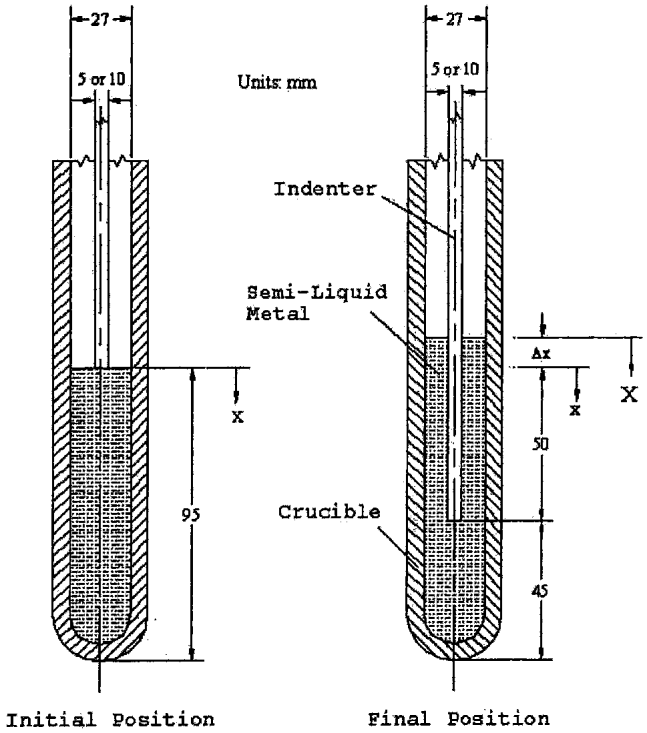

Fig. 7 Initial and final positions of penetration tool

the indenter or punch is moved back to its starting position. Positions of the indenter or punch during testing are shown in Fig. 7.

In metal forming, if the ratio of the workpiece diameter (D) to the penetration tool diameter (d) is larger than five, the associated forming process should be designated as indentation. When the ratio is smaller than five, the process becomes piercing or back extrusion (Ref 10). In the present experiment, the inside diameter of the crucible, or the workpiece diameter (D), is 27 mm. Two penetration tools are used: one has a diameter (d) of 5 mm while the other has a diameter of 10 mm. Since the corresponding ratios are 5.4 and 2.7, respectively, the former can be considered as an indentation process, while the later is a piercing process. As a result, the 5 mm diameter tool is named an indenter and the 10 mm one is called a punch.

4. Results and Discussion

Four sets of testing conditions were conducted. For the first two sets of tests, the 5 mm diameter indenter (d) was used, and the 10 mm diameter punch was used for the last two sets. The first two cases are under indentation deformation, and the later two cases are piercing forming. Both the indenter and punch tools were lowered at two different velocities until they reached a depth of 50 mm in the steel sample, as shown in Fig. 7.

During testing, the penetration forces and the corresponding penetration positions are recorded. The forces are then normalized by the cross section of the indenter or punch and the peak flow stress (Y) near the solidus temperature. Based on correlation of Eq 1, the peak stress at the solidus temperature can be found to be 8.5 MPa. This value (8.5 MPa) is used to normalize the indentation and piercing forces. Based on the tool positions

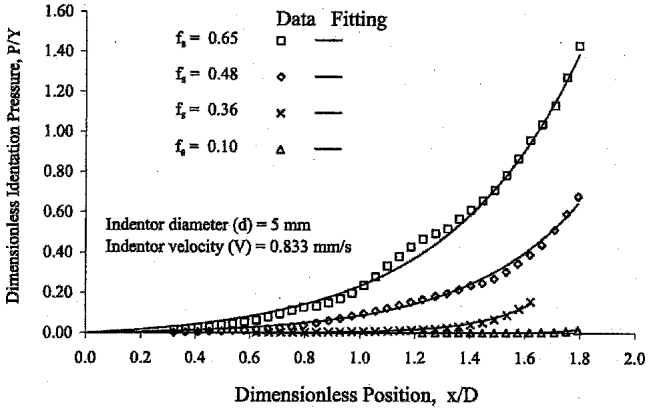

Fig. 8 Relationship between indentation pressure and depth using 5 mm indenter at 0.833 mm/s loading rate (Case 1)

recorded, the normalized penetration depth (X) defined in Fig. 7 can be found as:

$$X = x/D + (x/D)\,(\mathrm{d}/D)^2 \qquad \text{(Eq 2)}$$

where x is the coordinate measured from the originally initial contact position (Fig. 7), and D, the crucible diameter equal to 27 mm, is used for normalization. It is noteworthy that, as shown in Fig. 7, when the tool continues to pierce into the crucible, an equal amount of material in the crucible will be squeezed upwards. As a result, the penetrated depth (X), or contact length between the tool and the mushy-state material, increases and should be modified according to Eq. 2.

Figure 8 shows the results of the normalized indention pressure for the first case, i.e., a 5 mm diameter indenter loaded at a speed (V) of 0.833 mm/s (50 mm/min). As shown, samples were examined at four different temperatures ranging from 1410 to 1450 °C. The corresponding solid fraction varies from 10 to 65%. As shown, the indentation pressure grows exponentially as the depth of the indentation increases. Results also indicate that the pressure increases as the solid fraction enlarges or as the testing temperature decreases.

After examination of the data, a correlation of the dimensionless indentation pressure (P/Y) with respect to the solid fraction (f_s) and normalized penetration depth (X) can be found as:

$$\frac{P}{Y} = (\mathrm{A} + \mathrm{B}f_s)e^{CX} \qquad \text{(Eq 3)}$$

where A, B, and C are dimensionless correlation constants. In this case, A and B are −0.0428 and 0.1136, respectively, while C has a different value for different solid fractions (f_s), as listed in Table 2. It should be noted that the friction behavior between the tool (indenter) and the workpiece is very complicated even for fully solidified materials. Most indentation and piercing problems studied only consider the initial contact pressure without including the interface friction (Ref 11, 12). As a result, it is extremely difficult, if not impossible, to find a relatively simple relationship to correlate the constant C with the solid fraction. In the current study, a separate constant is given for each solid fraction considered.

The predictions based on the correlation of Eq 3 for four different solid fractions are plotted in Fig. 8. As shown, the

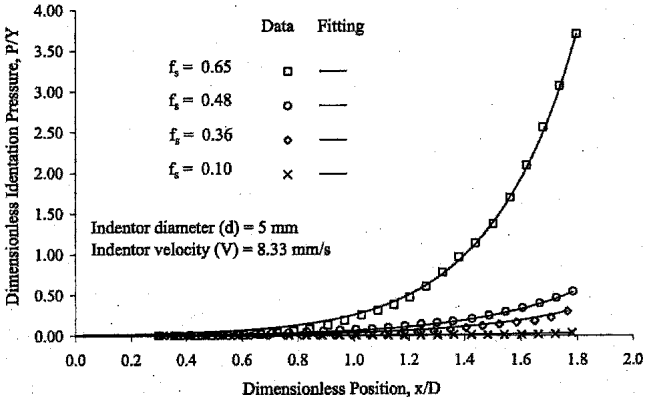

Fig. 9 Relationship between indentation pressure and depth using 5 mm indenter at 8.33 mm/s loading rate (Case 2)

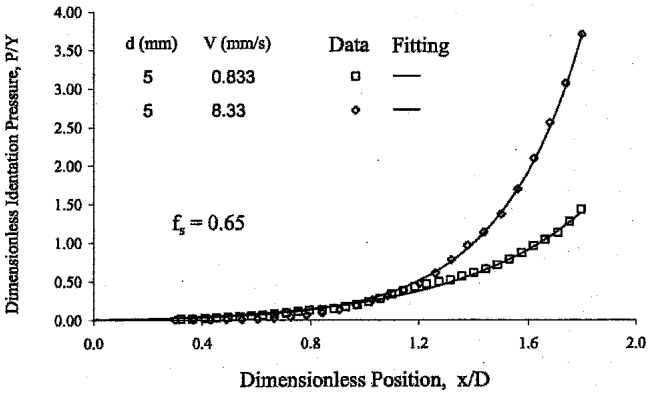

Fig. 10 Effects of indentation speed on indentation pressure for solid fraction at 0.65 (Cases 1 and 2)

Table 2 Correlation constants for indentation pressure

	F_s	A	B	C
Case 1, d = 5 mm,	0.65	-4.28×10^{-2}	0.1136	2.120
V = 0.833 mm/s	0.48	-4.28×10^{-2}	0.1136	2.454
	0.36	-4.28×10^{-2}	0.1136	5.117
	0.10	-4.28×10^{-2}	0.1136	10.927
Case 2, d = 5 mm,	0.65	-1.88×10^{-3}	1.51×10^{-2}	3.357
V = 0.833 mm/s	0.48	-1.88×10^{-3}	1.51×10^{-2}	2.699
	0.36	-1.88×10^{-3}	1.51×10^{-2}	2.689
	0.10	-1.88×10^{-3}	1.51×10^{-2}	2.376
Case 3, d = 10 m,	0.48	-7.05×10^{-7}	9.41×10^{-4}	3.1981
V = 0.833 mm/s	0.36	-7.05×10^{-7}	9.41×10^{-4}	2.849
	0.10	-7.05×10^{-7}	9.41×10^{-4}	2.104
Case 4, d = 10 m,	0.48	-1.65×10^{-4}	7.06×10^{-3}	2.814
V = 0.833 mm/s	0.36	-1.65×10^{-4}	7.06×10^{-3}	2.177
	0.10	-1.65×10^{-4}	7.06×10^{-3}	2.018

correlation equation fits the experimental data very well. The square of the correlation coefficients R^2 for the present data fitting is close to 0.8. The coefficient R is used to gage the correlation accuracy and always lies between −1 and +1. A value of zero occurs when the two variables, indentation pressure and depth, are totally independent of each other, while it reaches one when the indentation pressure and depth correlate perfectly, i.e., no deviation from the exponential curve (Ref 13). An R^2 value close to 0.8 means that Eq 3 agrees with the experimental data reasonably well.

In Case 2, the loading speed (V) is set at 8.33 mm/s or 500 mm/min. The penetration pressure versus penetration depth graph is shown in Fig. 9. The corresponding correlations are also depicted in the figure. As shown, the correlation fits the measurement data very well. The constants, A, B, and C used in the correlation are reported in Table 2. Comparing Fig. 8 to Fig. 9 shows that pressure is not sensitive to loading speed until the solid fraction is greater than 48%. For a 65% solid fraction, as shown in Fig. 10, the pressure more than doubles for indentations deeper than 1.5, as the loading speed increases from 0.833 to 8.33 mm/s. The insensitivity to the loading speed at a lower solid fraction is unexpected and this phenomenon is worthy of further investigation.

The corresponding piercing behavior is studied under the conditions of Cases 3 and 4. The test results of piercing pressures and depths are plotted in Fig. 11 and 12 at three different solid fractions for piercing velocities of 0.833 mm/s (Case 3)

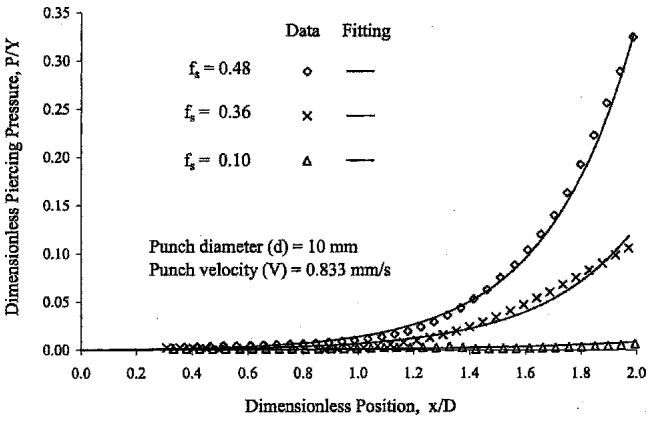

Fig. 11 Relationship between piercing pressure and depth using 10 mm punch at 0.833 mm/s loading rate (Case 3)

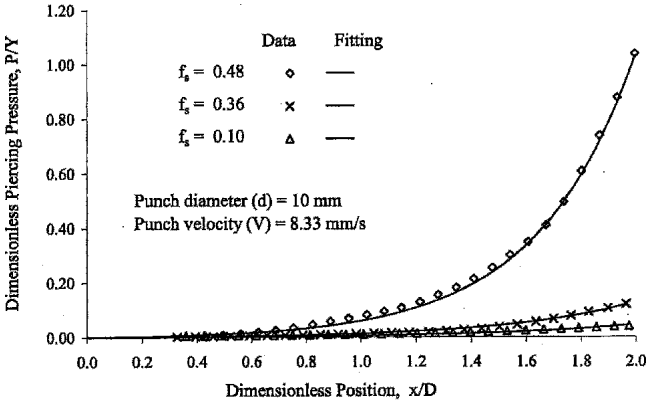

Fig. 12 Relationship between piercing pressure and depth using 10 mm punch at 8.33 mm/s loading rate (Case 4)

and 8.333 mm/s (Case 4), respectively. Again, the corresponding correlation constants, A, B, and C are summarized in Table 2. As shown, the piercing pressure grows exponentially as the penetration depth increases, which is similar to the indentation cases reported in Fig. 8 and 9, although the magnitude may be different. Also, similar to Fig. 10, Fig. 13 shows that at a higher solid fraction (f_s = 0.48), the piercing pressure increases by more than double as the loading speed increases from 0.833 to 8.33 mm/s. However, comparing Fig. 11 and 12, the insensi-

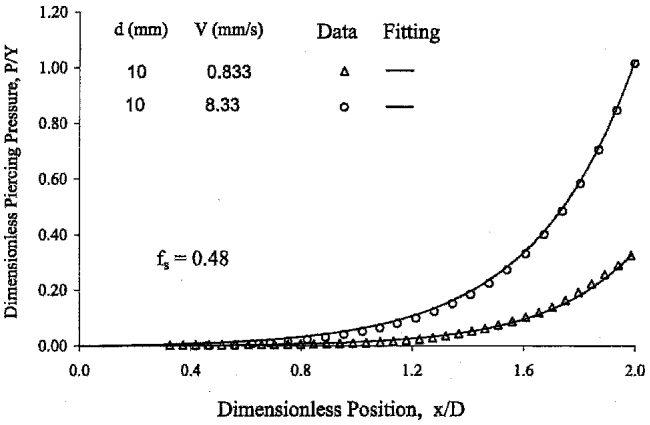

Fig. 13 Effects of indentation speed on piercing pressure for solid fraction at 0.48 (cases 3 and 4)

tivity of the loading speed to the piercing pressure at relatively low solid fractions (f_s = 0.36 and 0.10) is observed yet again.

Also, it is to be noted that for the cases using a larger penetration tool (10 mm in diameter) at a higher loading speed (500 mm/min), difficulties were experienced in maintaining a constant loading speed for a solid fraction larger than 50%. As a result, in Fig. 11 and 12, only those test conditions with a solid fraction less than 50% were reported.

5. Conclusions

The deformation behavior of steel in mushy states under the indentation and piercing forming conditions was studied. A hot penetration tester was developed to provide the flow stress data of steel at various mushy-states and different forming speeds. The tester was specifically designed to accommodate the high temperatures required to melt the steels. The correlation between the temperature and the percentage of the solid phase is used to define the characteristics of the mushy state.

The mushy states for the solid fraction between 0.10 and 0.65 were evaluated. It was observed that the indentation or piercing force increases quickly with the increasing content of the solid phase, which can often result in a failure of tools or punches. In fact, difficulties were experienced for piercing testing for a solid fraction larger than 50% at a higher loading speed (500 mm/min). In piercing, a larger penetration tool (10 mm in diameter) is used. Consequently, the hot piercing test is more suitable for a metal sample having relatively low solid content.

All results indicate the penetration pressures of steels in mushy states are highly dependent on the solid phase percentage and forming speed in both indentation and piercing tests. The penetration pressure grows exponentially as the depth of the indentation or piercing increases. Results also indicate the pressure increases as the penetration speed increases. The forming pressure can double if the loading speed increases one order of magnitude. Correlations were developed among the penetration speed, solid fraction, and tool traveling position. The correlation developed here can be conveniently used for comparison of the force or energy of present processes with those of other forming processes.

It should also be noted that at relatively low-solid fractions (less than 0.36), the insensitivity of the loading speed to the penetration pressure was observed in both indentation and piercing tests. The reason for this insensitivity is still not fully understood. Also, the influence of the penetration speed and the solid fraction on the penetration force or loading is being evaluated. The flow stress-strain data reported in Eq 1 are used as input to the analytical correlation and the present experimental data can be used for verification and refinement of the further analytical study.

Acknowledgments

The authors gratefully acknowledge support of this research by the U.S.-Czechoslovak Science and Technology Program under Grant No. 94-045 through U.S. National Institute of Standards and Technology, and by the U.S. National Science Foundation under Grant No. DMI-9696062 and DMI-9812984. Also, the assistance from Dr. B.S. Zhao of Arizona State University for data analyses is greatly appreciated.

References

1. M.C. Flemings, Behavior of Metal Alloys in the Semisolid State, *Metall. Trans. B,* Vol 22B, 1991, p 269-293
2. M. Kiuchi, Metal Forming in Mushy State, in *Plasticity and Modern Metal-Forming Technology,* T.Z. Blazynski, Ed., Elsevier Applied Science, 1989, Chap. 11, p 289-313
3. T.Z. Kattamis and T.J. Piccone, Rheology of Semisolid Al-4.5%Cu-1.5%Mg Alloy, *Mater. Sci. Eng.,* Vol A131, 1991, p 265-272
4. M. Kiuchi and S. Sugizama, A New Process to Manufacture Semi-Solid Metals, *Proceedings of 2nd Int. Conf. on the Semi-Solid Processing Alloys and Composites,* S. Brown and M.C. Flemings, Ed., 1992, p 47-56
5. P. Kumar, C.L. Martin, and S. Brown, Shear Rate Thickening Flow Behavior of Semisolid Slurries, *Metall. Trans. A,* Vol 24A, 1993, p 1107-1116
6. A.K. Dahle and L. Arnberg, The Rheological Properties of Solidifying Aluminium Foundry Alloys, *JOM,* Vol 48 (No. 3), 1996, p 34-37
7. M.G. Worster, Convection in Mushy Layers, *Ann. Rev. Fluid Mech.,* Vol 29, 1997, p 91-122
8. *Metals Handbook,* Desk Ed., H.E. Boyer and T.L. Gall, Ed., American Society for Metals, 1985, Chap. 28
9. A.A. Tseng, J. Horsky, M. Raudensky, and P. Kotrbace, Deformation Behavior of Steels in Mushy State, *Mater. Design,* 2001, Vol 22 (No. 2), p 83-92
10. W.A. Backofen, *Deformation Processing,* Addison-Wesley, 1972
11. W.F. Hosford and R.M. Caddel, *Metal Forming: Mechanics and Metallurgy,* 2nd ed., PTR Prentice Hall, Englewood Cliffs, NJ, 1993
12. F.H. Lin and A.A. Tseng, A Finite Element Analysis of Elasto-Plastic Contact Problems in Metal Forming, *Mater. Design,* Vol 19 (No. 3), 1998, p 99-108
13. H.W. Coleman and W.G. Steele, *Experimentation and Uncertainty Analysis for Engineers,* John Wiley & Sons, 1989